Dynamic Analysis Model of Embedded Fluid Elastomeric Damper for Bearingless Rotor

Wu Shen[1,2], *Yang Weidong*[1*], *Li Ruirui*[1]

1. National Key Laboratory of Rotorcraft Aeromechanics, Nanjing University of Aeronautics and Astronautics, Nanjing 210016, P. R. China;

2. China Ship Scientific Research Center, Wuxi 214082, P. R. China

(Received 6 June 2015; revised 24 October 2015; accepted 9 December 2015)

Abstract: According to the structural characteristics of embedded fluid elastomeric damper and dynamic modeling method of bearingless rotor (BR) system, a time-domain dynamic model based on multilayer elastomeric theory and fluid dynamic equations is developed. The parameters contained in the analysis model are identified by dynamic experiment data of embedded fluid elastomeric damper. The dynamic characteristics curves calculated through dynamic model are compared with those derived from experimental data. The consistent results illustrate that the model can describe the nonlinear relationship between stress and strain of embedded fluid elastomeric damper under different displacement amplitude and frequency. Due to the validity and reliability of the dynamic analysis model, it can be used in aeroelastic characteristics calculation of BR with embedded fluid elastomeric damper for helicopters.

Key words: helicopter; bearingless rotor (BR); embedded fluid elastomeric damper; nonlinear dynamics characteristics

CLC number: V216.2 **Document code**: A **Article ID**: 1005-1120(2016)05-0552-07

0 Introduction

Bearingless rotor (BR) has made a great breakthrough in helicopter rotor technology, since it can replace flap, lead-lag and pitch hinges of conventional rotor by a flexbeam configuration[1]. Owing to simplification of rotor hub parts, BR has notable advantages in improving fatigue strength, reducing hub weight and depressing maintenance cost. Generally, BR systems utilize soft-in-plane design to reduce hub loads. As a result of that, small structural damping of flexbeam in lead-leg motion may result in aeromechanical instabilities for BR system, e. g. ground and air resonance[2,3]. Therefore, BR system needs extra damping in plane to enhance system stabilities.

Most modern soft-in-plane helicopter rotors are equipped with lead-lag dampers to alleviate aeromechanical instabilities. Popular lead-lag dampers include hydraulic damper, cylinder or plate elastomeric damper and cylinder fluid elastomeric damper[4,5]. However, these conventional lead-lag dampers are impractical in BR system. BR system is consisted of hub, blade and fleaxbeam surrounded by the torque tube. The inner and outer end of the fleaxbeam is connected with the hub and blade, respectively. The special configuration of BR system may lead to ineffective working for conventional structures of lead-leg damper. To overcome this problem, embedded elastomeric damper (EED) or embedded fluid elastomeric damper (EFED) is successfully developed for the lead-lag damper of BR system[6]. EED is a multiple lamination of metallic and elastomeric layers. It can shear and provide damping through energy dissipation along with the blade lead-lag motion. Moreover, EFED introduces additional damping from viscous liquid flowing rela-

* Corresponding author, E-mail address: ywdae@nuaa.edu.cn.

How to cite this article: Wu Shen, Yang Weidong, Li Ruirui. Dynamic analysis model of embedded fluid elastomeric damper for bearingless rotor[J]. Trans. Nanjing Univ. Aero. Astro., 2016,33(5):552-558.
http://dx.doi.org/10.16356/j.1005-1120.2016.05.552

tively to EED, which can supply larger damping.

Otherwise, the introduction of flexbeam configuration and larger elastic distortion of blade to the BR system can aggravate aerodynamic coupling problems[7]. Precise dynamic model of the BR system should be developed for aeroelastic stability analysis. Generally, a direct integral method is introduced to solve lead-lag damper/rotor blade coupling motion in aeroelastic characteristics calculation[8, 9]. According to the requirement of dynamic modeling and calculating method for BR system, the damper should be modeled as an individual part that can integrate easily with dynamic equations of the blade motion[10]. Familiar models of lead-lag damper cannot reflect nonlinear dynamic characteristics accurately, because they are always established in frequency domain[11]. Though fractional time derivative model can be used in time domain calculation, and the model needs inverse Laplace transforms, leading to low efficiency. Therefore, it is necessary to develop a dynamic analysis model for valid description of the relationship between stress and stain in time domain for the lead-leg damper of BR system.

A dynamic analysis model of EFED with several parameters will be established according to the multilayer configuration and work principle of EFED. The dynamic experiments have been carried to research the dynamic characteristics of EFED and identify the model parameters. Furthermore, the curves calculated by dynamic model are compared with those derived from test to ensure the validity and reliability of dynamic analysis model for EFED.

1 Configuration of EFED

As shown in Fig. 1, each blade of the helicopter BR system is equipped with a pair of EFEDs[12]. The paired lag dampers are interconnected by a shear restraint. Both damper tops are connected with the root of the torque tube through the shear restraint, and both bottoms are joined directly with the flexbeam. Furthermore, EFEDs can restrain the relative motion between

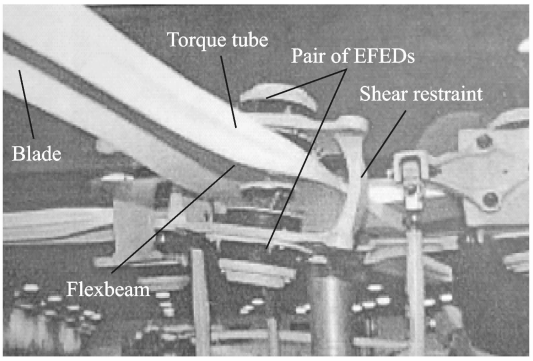

Fig. 1 Schematic of helicopter BR blade with paired EFEDs

the flexbeam and torque tube providing lead-leg damping to the BR system.

Fig. 2 shows a section view of EFED. The flexible body of the damper is a multiple lamination made up of crossbedded metallic and elastomeric annular layer. A cavity is formed by the lamination, top and bottom plate. In the middle of the cavity, a rectangular separate plank is combined to the bottom plate, dividing the cavity into two chambers. The chambers are connected with each other only by two narrow channels composed of the lamination and separate plank. Additionally, there are two holes on the top plate of EFED. Through the holes, viscous fluid can be filled and drained into EFED.

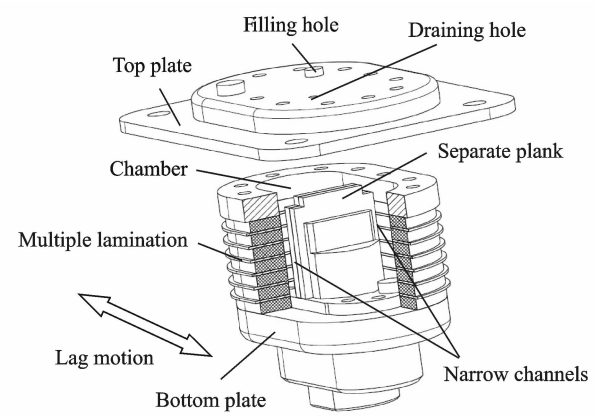

Fig. 2 Section view of EFED configuration

Under lag excitation, the top and the bottom plate move oppositely along the lag direction (Fig. 2), inducing sheared distortion for elastomeric materials and viscous fluid flowing through the narrow channels. They can provide stiffness

and damping for the lag motion of the rotor blade.

2 Dynamic Model of EFED

Because of different work principles of providing damping, dynamic analysis model should be developed for multiple elastomeric materials and viscous liquid in EFED, respectively.

2.1 Dynamic model of elastomeric material

In the helicopter rotor system, lag motion of the blade is always in the low frequency region. With the low frequency, the inertial force generated from metallic shims of the lamination is small, so that the influence of metallic layers on the dynamic characteristics can be ignored[13].

Fig. 3 schematically shows the dynamic model of multiple elastomeric material which includes several internal anelastic displacement fields (ADF) and friction-spring pairs[14]. As shown in Fig. 3, multiple friction-damping and linear-spring elements are in parallel with the nonlinear multi-ADF model.

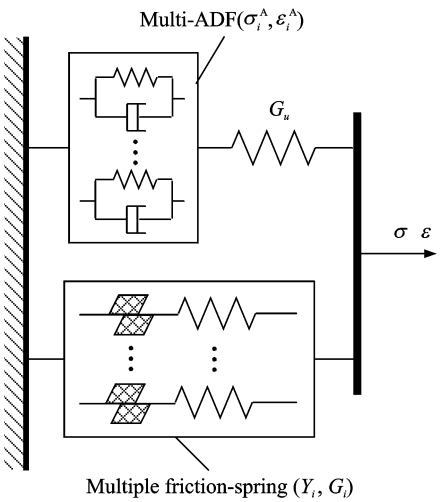

Fig. 3 Schematic of multiple elastomeric materials

The constitutive equations of multiple elastomeric materials are given by

$$\sigma = G_u\left(\varepsilon - \sum_{i=1}^{n}\varepsilon_i^{\mathrm{A}}\right) + \sum_{j=1}^{m}\sigma_j^{\mathrm{f}} \tag{1}$$

$$\sigma_i^{\mathrm{A}} = G_u(\varepsilon - c_i\varepsilon_i^{\mathrm{A}}) \tag{2}$$

$$\frac{c_i G_u}{\Omega_i}\dot{\varepsilon}_i^{\mathrm{A}} = \sigma_i^{\mathrm{A}} + \frac{c_i G_u}{\Omega_i}k_{di}(\sigma^{\mathrm{A}})^3 \tag{3}$$

where G_u is the shear modulus. The total shear strain ε and the anelastic shear strain ε^{A} are coupled by the parameterc. σ, σ^{A} and σ^{f} represents the total, anelastic and friction-spring stress, respectively. n, m are the amount of ADFs and friction-spring pairs, respectively, and Ω, k_d the parameter of frequency and viscous force, respectively.

Each of the friction-spring stress σ^{f} is determined by a trial stress σ_t, as shown in

$$\sigma_t = \sigma_j^{\mathrm{f}} + G_j \times (\varepsilon_{j+1} - \varepsilon_j) \tag{4}$$

$$\sigma_{j+1}^{\mathrm{f}} = \begin{cases} \sigma_t & |\sigma_t| < Y_j \\ (\sigma_t/|\sigma_t|) \times Y_j & |\sigma_t| \geqslant Y_j \end{cases} \tag{5}$$

where the parameters Y and G represents associated yield stress of friction and stiffness of spring element, respectively.

2.2 Dynamic model of viscous liquid

As shown in Fig. 4, viscous liquid in the cavity of EFED flows in the channel of mutative diameter providing damping through energy dissipation[15]. In Fig. 4, D and d denote the section diameter of wide and narrow channel, respectively. l represents the length of narrow channel.

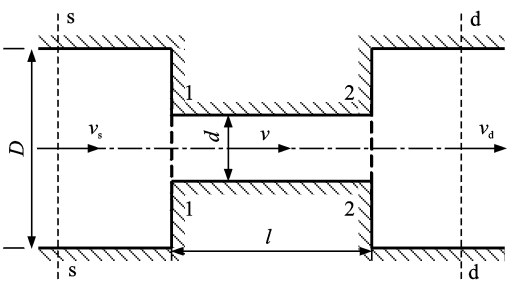

Fig. 4 Schematic of viscous liquid flowing

Based on the momentum principle and Bernoulli's equation, dynamic equations of viscous liquid are given by

$$\begin{cases} \dfrac{p_s}{\rho g} + \dfrac{\alpha_s v_s^2}{2g} = \dfrac{p_2}{\rho g} + \dfrac{\alpha_2 v_2^2}{2g} + \Sigma\zeta\,\dfrac{v_2^2}{2g} \\ \rho A_d v_d(\beta_2 v_2 - \beta_d v_d) = (p_d - p_2)A_d \end{cases} \tag{6}$$

where p and v are the pressure and velocity of each section, respectively. ρ denotes the density and A the section area. α and β represent correction coefficient of kinetic energy and momentum.

The pressure difference of liquid flowing from s-s section to d-d section is given by

$$\Delta p = p_s - p_d = \left(\lambda\,\frac{l}{d} + \zeta_1 + \zeta_2\right)\rho\,\frac{v^2}{2} \tag{7}$$

where λ and ζ are damping coefficients.

The damping force F_L resulted from viscous liquid flowing is given by

$$F_L = c_e v_s^2 \tag{8}$$

$$c_e = \frac{\rho}{8}\frac{\pi D^6}{d^4}\left(\lambda\frac{l}{d}+\zeta_1+\zeta_2\right) \tag{9}$$

2.3 Dynamic model of EFED

According to the dynamic characteristics of multiple elastomeric material and viscous liquid, the global equation of EFED motion is given as follows

$$M\ddot{\boldsymbol{u}} + K\boldsymbol{u} = F - F_E - F_L \tag{10}$$

where $\boldsymbol{u}$ is the global displacement vector.

The established dynamic model of EFED includes several parameters that are identified by the dynamic test of EFED. To solve the integrated vibration equation, the equation should be transformed into first-order ordinary differential equation by the order reduction method. Finally, a direct integral method of fourth-order Runge-Kutta is used to solve the above equation.

3 Dynamic test of EFED

3.1 Test details

The EFED test have 7 layers of elastomeric rubber and 6 layers of metallic flakes in the lamination. Main parameters of EFED are shown in Table 1 and photos of the EFED test are shown in Fig. 5.

Table 1 Main parameters of EFED test

Structural parameter	Value
Thickness of elastomeric layer/ mm	4.5
Shearing area of elastomeric layer/ mm^2	4 700
Thickness of metallic layer/ mm	1.5
Height of separate plank/ mm	4.4
Width of separate plank/ mm	4.0
Thickness of separate plank/ mm	6.0
Width of narrow channel/ mm	1.0

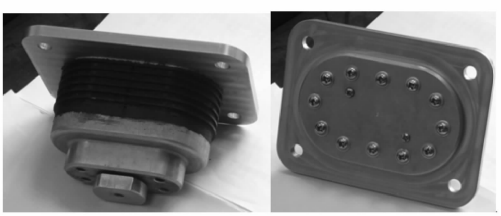

Fig. 5 EFED test

The equipment and instrument of the test include signal generator, power amplifier, exciter, charge amplifier, force sensor, displacement sensor and signal collection device. The connection of the above equipments is schematically shown in Fig. 6 and the actual photo of test equipments is shown in Fig. 7.

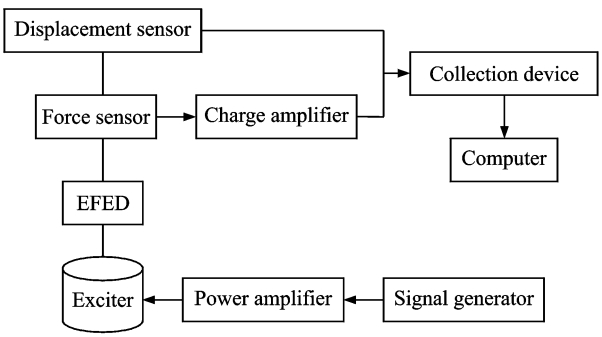

Fig. 6 Schematic of test system

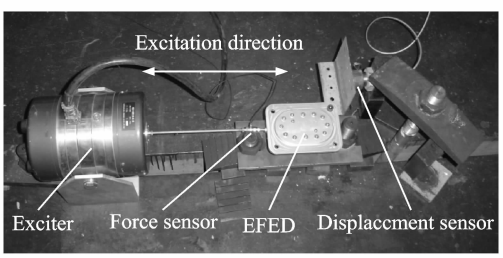

Fig. 7 Dynamic test of EFED

The exciter of the dynamic experiment is actively operated by the signal generator. Under the different excitation signals, e. g. sine wave, EFED can move back and forth in the excitation direction. Force and displacement signals of the EFED test with different frequency or displacement amplitude can be collected by the force and displacement sensors. Through the collection and processing device, EFED test results of the force and displacement are transported to the computer.

3.2 Test results and discussion

Hysteresis loops (time history of force versus displacement) of EFED and EED (without filling viscous oils) under different displacement amplitude at 4 Hz are plotted in Fig. 8, respectively.

It is seen that hysteresis loops of EFED are more elliptical than those of EED. The areas sur-

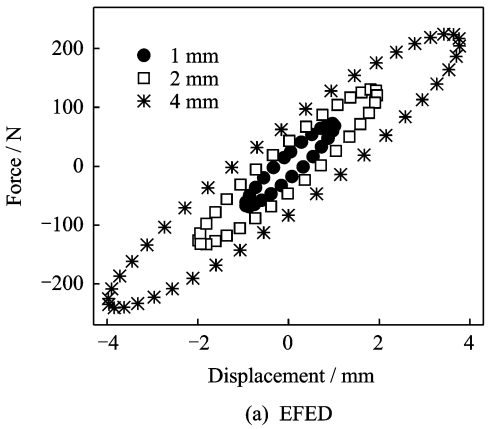

(a) EFED

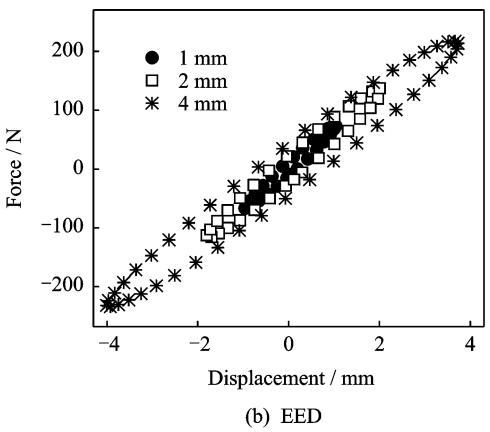

(b) EED

Fig. 8 Hysteresis loops at 4 Hz

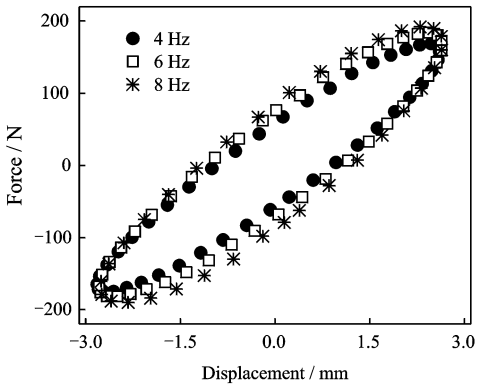

(a) EFED

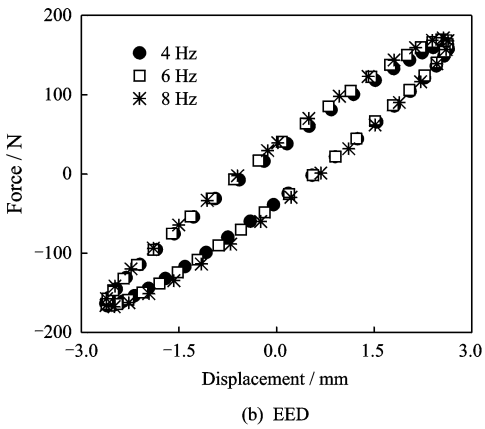

(b) EED

Fig. 9 Hysteresis loops at 2.8 mm

rounded by the elliptical curves of EFED and EED all increase notably with the displacement amplitude of excitation increasing. It is demonstrated that the change of displacement has an evident effect on dynamic characteristics of these dampers.

Moreover, the area of EFED under the same displacement amplitude is larger than that of EED, suggesting that the ability of energy dissipated for EFED is stronger than EED. Furthermore, the slopes of the major axes of the ellipses are parallel, indicating that the stiffness of EFED is constant. While in the case of EED, the slopes are variable under different displacement amplitude. It is demonstrated that the stiffness of EED will decrease with the amplitude of excitation increasing.

Hysteresis loops of EFED and EED under different frequency at 2.8 mm are plotted in Fig. 9, respectively. Compared with the change of hysteresis loops under different displacement amplitude, the change of shape and area surrounded by hysteresis loops with different frequency is insignificant. The areas and slopes of the elliptical curves increase by a small range with the frequency of excitation increasing. It suggests that dynamic properties of EFED and EED are not sensitive to the frequency.

According to the analysis on the dynamic characteristics of EFED and EED with amplitude and frequency changing, more stable dynamic property and stronger energy dissipated ability of EFED can be evidently displayed.

4 Model Validation

To prove the validity of the established EFED model, it is necessary to identify the model parameters first. According to the genetic algorithm of parameter identification in Ref. [16] and dynamic test data of EFED in the latest section, the identified model parameters are shown in Table 2.

Hysteresis loops comparison under different displacement amplitude at 6 Hz and different fre-

quency at 2 mm calculated with the EFED model and test data are plotted in Figs. 10, 11, respectively.

Table 2 Identified model parameters

Model parameter	Value
$\rho/(\mathrm{kg \cdot m^{-3}})$	928
G_u/MPa	0.77
$c_e/(\mathrm{N \cdot s \cdot m^{-1}})$	20
c_1	4.3
c_2	5.17
c_3	3.36
$k_{d1}/(\mathrm{Hz \cdot Pa^{-3}})$	1.04×10^{-16}
$k_{d2}/(\mathrm{Hz \cdot Pa^{-3}})$	4.12×10^{-14}
$k_{d3}/(\mathrm{Hz \cdot Pa^{-3}})$	1.93×10^{-11}
Y_1/Pa	917
Y_2/Pa	170
Y_3/Pa	288
G_1/MPa	1.33
G_2/MPa	0.189
G_3/MPa	0.146
Ω_1/Hz	0.01
Ω_2/Hz	0.58
Ω_3/Hz	19

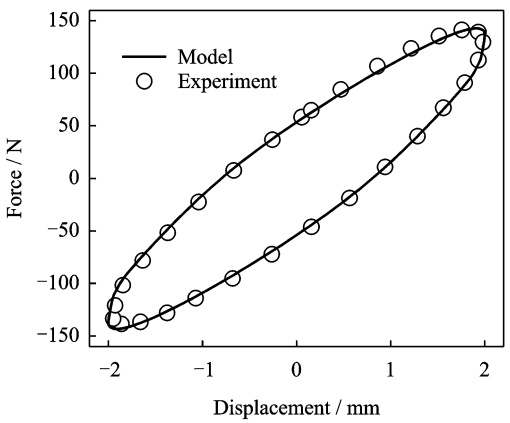

Fig. 10 Comparison of hysteresis loops at 6 Hz

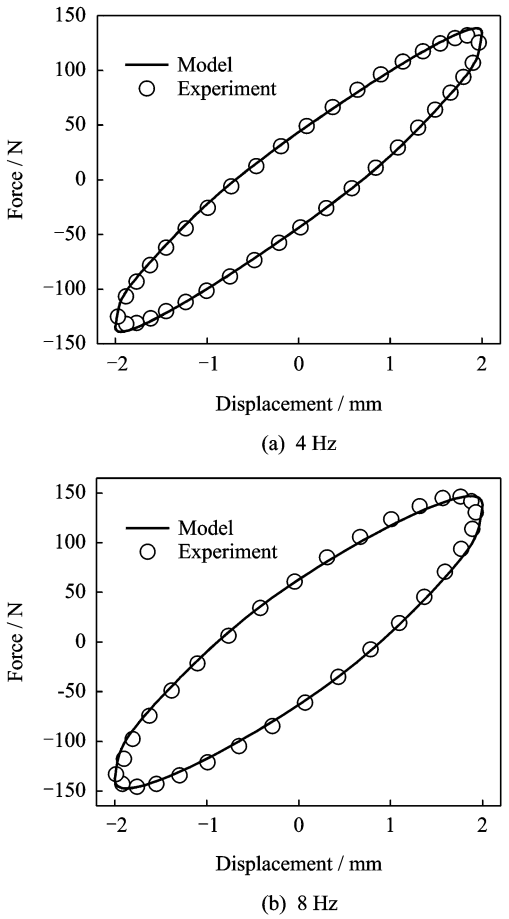

Fig. 11 Comparison of hysteresis loops at 2 mm

Compared with the curves calculated from the EFED model and test data, it is tiny difference between them. It suggests that the dynamic model of EFED can exactly describe the nonlinear relationship between force and displacement at different frequency and displacement amplitude. Therefore, the dynamic analysis model can reflect the nonlinear dynamic properties of EFED with high precision.

5 Conclusions

(1) Compared with EED, EFED possesses more complex configuration, but more stable dynamic property and stronger energy dissipated ability.

(2) The dynamic analysis model which is developed on the multilayer of elastomeric rubber configuration and dynamic equations of viscous fluid is valid and reliable, suggesting that the es-

tablished model can exactly describe the nonlinear dynamic characteristics of EFED.

(3) The EFED model that can be integrated into dynamic equations of BR system is convenient for the aeroelastic stability analysis of the helicopter BR system.

References:

[1] DIXON P, BISHOP H E. The bearingless main rotor[J]. Journal of the American Helicopter Society, 1980, 25(3): 15-21.

[2] PANDA B, MYCHALOWYCZ E. Aeroelastic stability wind tunnel testing with analytical correlation of the Comanche bearingless main rotor[J]. Journal of the American Helicopter Society, 1997, 42(3): 207-217.

[3] ZIABARI M Y, GHADIRI B. Vibration analysis of elastic uniform cantilever rotor blades in unsteady aerodynamics modeling[J]. Journal of the Aircraft, 2010, 47(4): 1430-1435.

[4] HU W, WERELEY N, CHEMOUNI L. Semi-active linear stoke magnetorheological fluid-elastic damper for helicopter main rotor blades[J]. Journal of Guidance, Control and Dynamics, 2007, 30(2): 565-575.

[5] WU Shen, YANG Weidong. Model experiment on nonlinear dynamic characteristics of rotor fluidlastic damper[J]. Journal of Nanjing University of Aeronautics & Astronautics, 2011, 43(3): 318-323. (in Chinese)

[6] PANDA B, MYCHALOWYCZ E, TARZANIN F J. Application of passive dampers to modern helicopters [J]. Smart Materials and Structures, 1996, 5(5): 509-516.

[7] LIM I G, LEE I. Aeroelastic analysis of bearingless rotors using large deflection beam theory[J]. AIAA Journal, 2007, 45(3): 599-606.

[8] LIM I G, LEE I. Aeroelastic analysis of bearingless rotors with a composite flexbeam [J]. Composite Structure, 2009, 88: 570-578.

[9] YU Zhihao, YANG Weidong, DENG Jinghui. Model of rotor aeroelastic stability using dynamic of flexible multibody system[J]. Journal of Aerospace Power, 2012, 24(5): 1122-1130. (in Chinese)

[10] HU W, WERELEY N. Distributed rate-dependent elastoslide model for elastomeric lag dampers [J]. Journal of Aircraft, 2007, 44(6): 1972-1984.

[11] HU Guocai, HOU Zhiqiang. An improved nonlinear VKS model of elastomeric lag damper based on its complex modulus[J]. Engineering Mechanics, 2005, 22(S): 73-77. (in Chinese)

[12] NGATU G, HU W, WERELY N M. Adaptive snubber type magnetorheological fluid elastomeric helicopter lag damper[J]. AIAA Journal, 2010, 48 (3): 598-610.

[13] LI Ruirui, YANG Weidong, YU Zhihao. Multiple parameters dynamic modeling and analysis of helicopter rotor multi-layer elastomeric damper[J]. Journal of Aerospace Power, 2014, 29(4): 844-851. (in Chinese)

[14] BRACKBILL C, LESIEUTRE G. Characterization and modeling of the low strain amplitude and frequency dependent behavior of elastomeric damper materials[J]. Journal of the American Helicopter Society, 2000, 47(1): 34-42.

[15] LU Minxun, LI Wanli. Hydrodynamics and fluid drive[M]. Shanghai: Tongji University Press, 2006: 17-36. (in Chinese)

[16] WU Shen. Research on dynamic characteristics of helicopter rotor fluid-elastomeric damper[D]. Nanjing: Nanjing University of Aeronautics & Astronautics, 2014. (in Chinese)

Dr. **Wu Shen** received Ph. D. degree in aircraft design from Nanjing University of Aeronautics and Astronautics (NUAA) in June 2014. He joined in China Ship Scientific Research Center (CSSRC) in August 2014, where he was a senior engineer of key laboratory on ship vibration and noise. His research is focused on rotor dynamics, vibration control and ship propeller design.

Prof. **Yang Weidong** received Ph. D. degree in aircraft design from Nanjing University of Aeronautics and Astronautics (NUAA) in 1995. He joined in Nanjing University of Aeronautics and Astronautics (NUAA) in July 1995, where he was a professor of national key laboratory of rotorcraft aeromechanics. His research is focused on flight dynamics, rotor dynamics, active and passive vibration control.

Dr. **Li Ruirui** received Ph. D. degree in aircraft design from Nanjing University of Aeronautics and Astronautics (NUAA) in 2015. His research is focused on elastomeric damper design and rotor vibration control.

(Executive Editor: Xu Chengting)